Article

A Dual Integral Equation Approach for Evaluating the Shielding of Thick Circular Disks against a Coaxial Loop

Giampiero Lovat [1],* , **Paolo Burghignoli [2]**, **Rodolfo Araneo [1]** and **Salvatore Celozzi [1]**

1 Electrical Engineering Division of DIAEE, University of Rome "Sapienza", Via Eudossiana 18, 00184 Rome, Italy
2 Department of Information Engineering, Electronics and Telecommunications, University of Rome "Sapienza", Via Eudossiana 18, 00184 Rome, Italy
* Correspondence: giampiero.lovat@uniroma1.it

Abstract: The electromagnetic interaction between a circular disk with finite conductivity and finite thickness and a coaxial circular loop of constant current is addressed here. The finite conductivity and thickness of the material disk lead to the adoption of suitable generalized boundary conditions, and the problem is thereby reduced to the solution of two sets of dual integral equations in the Hankel transform domain. Such equations are then solved by expanding the spectral unknowns in Neumann series of Bessel functions. An alternative formulation that is valid for purely conductive screens with no magnetic properties, which is computationally much faster, is proposed as well. The magnetic shielding effectiveness of the structure is studied in detail, pointing out its dependencies and possible critical situations.

Keywords: dual integral equations; electromagnetic shielding; regularizing Galerkin methods

1. Introduction

The interaction of electromagnetic fields with a circular disk (and its dual counterpart, i.e., a circular aperture in a plate) is a canonical problem in electromagnetic theory; research on this subject started in the 1950s and continues to attract the attention of the electromagnetic research community, although most studies have considered plane–wave excitation and/or perfectly-conducting (PEC) obstacles, ideally with zero thickness (see, e.g., [1–11]). In connection with this, we point out that in [12–14] the method of analytical preconditioning together with a Galerkin spectral Method of Moments with entire domain basis functions has been used to study the scattering from an infinitesimally thin PEC disk. Such a method has been adopted in those few studies which have considered thin disks, including those with dielectric properties [15–17]. On the other hand, the screening of a finite source (e.g., an electric or a magnetic dipole) by means of an infinite planar conductive shield is well-documented in both the frequency [18–20] and time [21,22] domains. Recently, the shielding of a thin conductive disk in the presence of an ideal vertical magnetic dipole has been studied in details [23]; however, the main assumption in [23] is that the disk thickness has to be smaller than the skin depth. Such an assumption introduces an upper limit in terms of frequency, and makes the formulation essentially into a low-frequency analysis. It is worth mentioning that the dual problem (i.e., a circular aperture in a thin metallic plate) has only recently been addressed [24]. In general, for thick disks (and as such for higher frequencies) analysis requires the adoption of generalized boundary conditions (GBCs). In turn, such GBCs require the introduction of both equivalent magnetic and electric current densities along the discontinuity interface [25–27]. This implies that, for thick disks an integral formulation based on GBCs leads to the derivation of two sets of dual integral equations (DIEs) to be solved.

In the present work, we solve such sets of DIEs (derived in the Hankel transform domain) by expanding the spectral unknowns in two Neumann series of Bessel functions.

Moreover, for thick metallic non-magnetic disks, a new generalized boundary condition is derived which is a generalization of that used for thin metallic screens. This means that it is sufficient to introduce only an equivalent surface electric current density as unknown. In this way, only one set of DIEs needs to be solved, thereby reducing the problem in a similar way to that of thin screens (preliminary results of this work have been presented in [28]). Thus, we generalize the analysis presented in [23] considering a finite source (a coaxial loop with finite radius and constant current) and a conductive disk with finite thickness, now without any limitation in frequency and thickness.

Finally, we want to mention a possible limitation of the present study. For simplicity, the electric current in the loop is assumed to be constant. In principle, the extension of the proposed analysis to non-constant currents could be feasible; however, introducing an azimuthal dependence of the exciting current would destroy the azimuthal invariance of the problem, thereby making the incident and scattered field hybrid. We leave this analysis for a future work.

It is clear that the focus of the paper is more on modeling than on the performance of different materials. We considered copper as a typical conductive material for the purpose of presenting numerical results that illustrate the proposed method; however, the validity of the method is general and has been tested on different values of the screen parameters.

The rest of this paper is organized as follows. The electromagnetic problem is described in Section 2, while in Section 3 the adopted Mitzner GBCs are discussed and two auxiliary sub-problems are introduced, each of which leads to DIEs for which the unknown is an equivalent spectral electric or magnetic current density. The procedure for the solution of these two sets of DIEs is outlined in Section 4, where all the quantities of interest are calculated as well. In Section 5, we propose a new boundary condition for thick conductive disks with no magnetic properties. This allows for formulating the problem in terms of only one set of DIEs, with consequent savings in terms of computation time compared with the original full formulation. In addition, we propose a series expansion (which in many practical case reduces to a single term) to efficiently evaluate the involved improper integrals. It is worth pointing out that the linear algebraic system resulting from the discretization of the involved DIEs defines a Fredholm problem, and as such has guaranteed convergence. Numerical results are presented in Section 6, showing the dependence of the magnetic shielding effectiveness on different geometrical parameters; these point out possible critical situations in particular configurations. Our conclusions are drawn in Section 7.

Finally, we want to clearly point out the contribution of the paper. The present manuscript addresses thick circular plates, and its novel contribution is twofold: (i) for general magneto-conductive plates, a set of established DIEs having both electric and magnetic currents as unknowns is solved rigorously, and (ii) for nonmagnetic conductive plates, an original alternative DIE formulation having only electric currents as unknowns is introduced. This allows an original and efficient tool to be derived, allowing for the evaluation of, e.g., the shielding effectiveness of material disks against a near-field source such as a circular current loop coaxial with the disk.

2. Formulation of the Problem

The configuration of the electromagnetic problem is shown in Figure 1, where a circular disk of thickness d and radius a with electrical conductivity σ and relative permeability $\mu_{\rm r}$ is reported. The disk is placed on the plane $z = 0$ of a cylindrical coordinate system (ρ, ϕ, z) with the center at the origin. The source of the electromagnetic field is a circular current loop of radius R and constant current I_0 coaxial with the disk and placed at $z = h$. The time-harmonic $e^{j\omega t}$ dependence is assumed and suppressed throughout. It should be noted that thanks to the azimuthal invariance of the problem the considered source produces a TE$_z$ field (with $E_\phi^{\rm inc}$, $H_\rho^{\rm inc}$, and $H_z^{\rm inc}$).
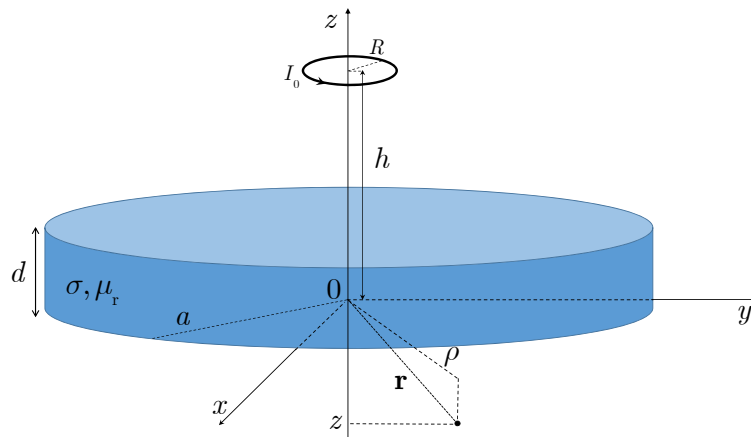
Figure 1. A circular disk of thickness d and radius a characterized by a conductivity σ and relative magnetic permeability μ_{r}, placed on the plane $z = 0$, in the presence of a current loop of radius R and constant current I_0 placed at $z = h$ and coaxial with the disk.

3. Pair of DIEs through Mitzner GBCs

The finite thickness of the screen makes the analysis more complex with respect to the infinitesimally-thin structure case. However, if the thickness d is sufficiently small (in particular, $k_0 d \ll 1$, where k_0 is the free-space wavenumber), it is possible to shrink the thickness to zero (reducing the screen to an infinitely thin surface) and adopt the Mitzner generalized boundary conditions (GBCs) [25]. The GBCs link the tangential electric and magnetic fields at the surface interfaces as

$$\frac{1}{2}\left[E_\phi(\rho, z = 0^+) + E_\phi(\rho, z = 0^-)\right] = \zeta_0 \hat{Z}_S(\mathbf{u}_z \times \mathbf{u}_\rho)\left[H_\rho(\rho, z = 0^+) - H_\rho(\rho, z = 0^-)\right] \tag{1}$$

and

$$\frac{1}{2}\left[H_\rho(\rho, z = 0^+) + H_\rho(\rho, z = 0^-)\right] = -\frac{\hat{Y}_S}{\zeta_0}(\mathbf{u}_z \times \mathbf{u}_\phi)\left[E_\phi(\rho, z = 0^+) - E_\phi(\rho, z = 0^-)\right], \tag{2}$$

where ζ_0 is the free-space impedance. Such GBCs have recently been used successfully in different scattering problems [16,17,27,29,30].

The coefficients $\hat{Z}_S$ and $\hat{Y}_S$ are related to the thickness and the electromagnetic parameters of the screen, and different expressions have been proposed in the literature. In his seminal paper [25], Mitzner derived

$$\hat{Z}_{SM} = \mathrm{j}\frac{\zeta_{\mathrm{cr}}}{2}\cot\left(\frac{k_{\mathrm{c}}d}{2}\right),$$

$$\hat{Y}_{SM} = \mathrm{j}\frac{1}{2\zeta_{\mathrm{cr}}}\cot\left(\frac{k_{\mathrm{c}}d}{2}\right) \tag{3}$$

with

$$k_{\mathrm{c}} = k_0\sqrt{\mu_{\mathrm{r}}\varepsilon_{\mathrm{cr}}},$$

$$\zeta_{\mathrm{cr}} = \sqrt{\frac{\mu_{\mathrm{r}}}{\varepsilon_{\mathrm{cr}}}}, \tag{4}$$

where $\varepsilon_{\mathrm{cr}} = 1 - \mathrm{j}\sigma/(\omega\varepsilon_0)$ indicates the relative complex permittivity.

It is worth noting that the condition $k_0 d \ll 1$ is not a limiting factor in all the practical configurations, where the thickness d of the screen is much smaller than the operating wavelength in air up to the microwave range.

The GBCs in (1) and (2) define a combined electrically resistive/magnetically conductive sheet with infinitesimal thickness, which supports both electric and magnetic surface currents that are related to the discontinuities across the sheet of the tangential magnetic and electric fields, respectively. Because any plane containing the vertical z-axis is an odd symmetry plane, the electric surface current density $\mathbf{J}_s$ is azimuthally directed, whereas the magnetic current density $\mathbf{M}_s$ is radially directed.

Following the same reasoning illustrated in [31], two sets of DIEs can be obtained in the canonical form

$$\int_0^\infty \gamma_i(\nu)\psi_i(\nu)\mathrm{J}_1(\nu r)\,\mathrm{d}\nu = h_i(r), \quad 0 \le r < 1 \tag{5}$$

$$\int_0^\infty \psi_i(\nu)\mathrm{J}_1(\nu r)\,\mathrm{d}\nu = 0, \quad r > 1, \tag{6}$$

where $r = \rho/a$, $\mathrm{J}_1(\cdot)$ is the Bessel function of order 1. The unknown functions are

$$
\begin{aligned}
\psi_1(\nu) &= \nu \tilde{J}_{S\phi}\left(\frac{\nu}{a}\right), \\
\psi_2(\nu) &= \nu \tilde{M}_{S\rho}\left(\frac{\nu}{a}\right),
\end{aligned} \tag{7}
$$

while the expressions of the functions γ_i ($i = 1, 2$) are

$$
\begin{aligned}
\gamma_1(\nu) &= \left(\frac{k_0 a}{2\lambda} + \hat{Z}_S\right), \\
\gamma_2(\nu) &= \left(\frac{\lambda}{2k_0 a} + \hat{Y}_S\right),
\end{aligned} \tag{8}
$$

and

$$
\begin{aligned}
h_1(r) &= -\frac{I_0 k_0 a R}{2} \int_0^\infty \frac{\mathrm{e}^{-\mathrm{j}\lambda|h|/a}}{\lambda} \mathrm{J}_1\left(\nu\frac{R}{a}\right)\mathrm{J}_1(\nu r)\nu\,\mathrm{d}\nu, \\
h_2(r) &= -\frac{I_0 R \zeta_0}{2} \int_0^\infty \mathrm{e}^{-\mathrm{j}\lambda|h|/a} \mathrm{J}_1\left(\nu\frac{R}{a}\right)\mathrm{J}_1(\nu r)\nu\,\mathrm{d}\nu.
\end{aligned} \tag{9}
$$

The functions $\tilde{J}_{S\phi}(\nu/a)$ and $\tilde{M}_{S\rho}(\nu/a)$ appearing in (7) are the Hankel transforms of order 1 of the surface current densities $J_{S\phi}(\rho)$ and $M_{S\rho}(\rho)$, respectively, while

$$\lambda = \sqrt{(k_0 a)^2 - \nu^2}$$

is the z-component of the normalized spectral wavenumber [31].

4. Solution of the Pair of DIEs

As described in [24], the $\psi_i(\nu)$ functions (which are related to either to the $\tilde{J}_{S\phi}$ or $\tilde{M}_{S\rho}$ functions) are expanded in Neumann series of Bessel functions, i.e.,

$$\psi_i(\nu) = \nu^{1-\mu_i} \sum_{n=1}^{+\infty} \psi_n^{(i)} \mathrm{J}_{2n-1+\mu_i}(\nu); \tag{10}$$

thus, thanks to the Weber–Schafheitlin integral ([32], 6.574.3), (6) is spontaneously satisfied. The parameters μ_i in (10) are arbitrary (provided that $\mu_i > 0$), and can be used to guarantee the convergence of the integrals arising in the analysis or to enforce a specific order of

singularity of the spatial currents at the edge of the aperture [24]. In fact, all the addends in (10) are the Hankel transforms of terms proportional to

$$r^2 \left(1 - r^2\right)^{\mu_i - 1} P_n^{(1,\mu_i-1)} \left(1 - 2r^2\right), \tag{11}$$

where $P_n^{(\cdot,\cdot)}(\cdot)$ are Jacobi polynomials of order n [33].

By using (10), (5) becomes

$$\sum_{n=1}^{+\infty} \psi_n^{(i)} \int_0^\infty \nu^{1-\mu_i} \gamma_i(\nu) J_1(\nu r) J_{2n-1+\mu_i}(\nu) \, d\nu = h_i(r), \tag{12}$$

which is valid for $0 \le r < 1$. By Galerkin testing (12), the dual integral equations are reduced to the matrix system

$$\sum_{n=1}^{+\infty} A_{mn}^{(i)} \psi_n^{(i)} = U_m^{(i)}, \qquad m = 1, \ldots, \tag{13}$$

where the matrix elements are provided by

$$A_{mn}^{(i)} = \int_0^\infty \nu^{1-2\mu_i} \gamma_i(\nu) J_{2m-1+\mu_i}(\nu) J_{2n-1+\mu_i}(\nu) \, d\nu \tag{14}$$

while it is easy to show that

$$U_m^{(1)} = -\frac{I_0 k_0 a R}{2} \int_0^\infty \nu^{1-\mu_i} J_{2m-1+\mu_i}(\nu) J_1\left(\nu \frac{R}{a}\right) \frac{e^{-j\lambda|h|/a}}{\lambda} \, d\nu \tag{15}$$

and

$$U_m^{(2)} = -\frac{I_0 R \zeta_0}{2} \int_0^\infty \nu^{1-\mu_i} J_{2m-1+\mu_i}(\nu) J_1\left(\nu \frac{R}{a}\right) e^{-j\lambda|h|/a} \, d\nu. \tag{16}$$

From (8) and (14), it can be immediately derived that to make the integrals convergent it must result $\mu_1 > 1/2$ and $\mu_2 > 1$; thus, we can set, e.g., $\mu_1 = 1$ and $\mu_2 = 3/2$, and the coefficients in (13) may be obtained as

$$\begin{aligned} A_{mn}^{(1)} &= \int_0^\infty \frac{\left(k_0 a + 2\lambda \hat{Z}_S\right)}{2\lambda \nu} J_{2m}(\nu) J_{2n}(\nu) \, d\nu, \\ A_{mn}^{(2)} &= \int_0^\infty \frac{\left(\lambda + 2k_0 a \hat{Y}_S\right)}{2k_0 a \nu^2} J_{2m+1/2}(\nu) J_{2n+1/2}(\nu) \, d\nu, \end{aligned} \tag{17}$$

i.e.,

$$\begin{aligned} A_{mn}^{(1)} &= \frac{k_0 a}{2} \int_0^\infty \frac{J_{2m}(\nu) J_{2n}(\nu)}{\lambda \nu} \, d\nu + \frac{\hat{Z}_S}{4m} \delta_{mn}, \\ A_{mn}^{(2)} &= \frac{1}{2k_0 a} \int_0^\infty \frac{\left(\lambda + 2k_0 a \hat{Y}_S\right)}{\nu^2} J_{2m+1/2}(\nu) J_{2n+1/2}(\nu) \, d\nu \end{aligned} \tag{18}$$

and the known terms in (13) as

$$\begin{aligned} U_m^{(1)} &= -\frac{I_0 k_0 a R}{2} \int_0^\infty J_{2m}(\nu) J_1\left(\nu \frac{R}{a}\right) \frac{e^{-j\lambda|h|/a}}{\lambda} \, d\nu, \\ U_m^{(2)} &= -\frac{I_0 R \zeta_0}{2} \int_0^\infty \frac{J_{2m+1/2}(\nu)}{\sqrt{\nu}} J_1\left(\nu \frac{R}{a}\right) e^{-j\lambda|h|/a} \, d\nu. \end{aligned} \tag{19}$$

By solving the algebraic system (13), the coefficients $\psi_n^{(i)}$ are derived and used to compute the spectral currents as

$$\tilde{J}_{S\phi}\left(\frac{\nu}{a}\right) = \sum_{n=1}^{+\infty} \psi_n^{(1)} \frac{J_{2n}(\nu)}{\nu} \tag{20}$$

and

$$\tilde{M}_{S\rho}\left(\frac{\nu}{a}\right) = \sum_{n=1}^{+\infty} \psi_n^{(2)} \frac{J_{2n+1/2}(\nu)}{\nu^{3/2}} \,. \tag{21}$$

From the knowledge of the spectral currents, any component of the field can easily be calculated. In particular, the z-components of the scattered magnetic fields $H_z^{(1)\text{scat}}$ and $H_z^{(2)\text{scat}}$ beyond the disk, (i.e., for $z < 0$) can be calculated as

$$H_z^{(1)\text{scat}}(r,z) = -\frac{\text{j}}{2a^2} \int_0^\infty \tilde{J}_{S\phi}\left(\frac{\nu}{a}\right) \frac{\text{e}^{-\text{j}\lambda|z|/a}}{\lambda} J_0(\nu r)\nu^2 \, \text{d}\nu \tag{22}$$

and

$$H_z^{(2)\text{scat}}(r,z) = -\frac{\text{j}}{2k_0\zeta_0 a^3} \int_0^\infty \tilde{M}_{S\rho}\left(\frac{\nu}{a}\right) \text{e}^{-\text{j}\lambda|z|/a} J_0(\nu r)\nu^2 \, \text{d}\nu, \tag{23}$$

i.e.,

$$H_z^{(1)\text{scat}}(r,z) = -\frac{\text{j}}{2a^2} \sum_{n=1}^{+\infty} \psi_n^{(1)} h_n^{(1)}(r,z) \tag{24}$$

and

$$H_z^{(2)\text{scat}}(r,z) = -\frac{\text{j}}{2k_0\zeta_0 a^3} \sum_{n=1}^{+\infty} \psi_n^{(2)} h_n^{(2)}(r,z) \tag{25}$$

with

$$h_n^{(1)}(r,z) = \int_0^\infty \frac{\nu}{\lambda} \, \text{e}^{-\text{j}\lambda|z|/a} J_0(\nu r) J_{2n}(\nu) \, \text{d}\nu \tag{26}$$

and

$$h_n^{(2)}(r,z) = \int_0^\infty \sqrt{\nu} \, \text{e}^{-\text{j}\lambda|z|/a} J_{2n+1/2}(\nu) J_0(\nu r) \, \text{d}\nu, \tag{27}$$

such that

$$H_z^{\text{scat}}(r,z) = H_z^{(1)\text{scat}}(r,z) + H_z^{(2)\text{scat}}(r,z)\,. \tag{28}$$

The z-component of the incident magnetic field (i.e., that radiated by the original current loop source in free space) is instead

$$H_z^{\text{inc}}(r,z) = -\text{j}\frac{I_0 R}{2a^2} \int_0^\infty \frac{\text{e}^{-\text{j}\lambda|z-h|/a}}{\lambda} J_1\left(\nu\frac{R}{a}\right) J_0(\nu r)\nu^2 \, \text{d}\nu\,. \tag{29}$$

From (28) and (29), the magnetic shielding effectiveness SE_H can easily be calculated through [34]:

$$\text{SE}_H = 20\log \frac{\left|H_z^{\text{inc}}(0,z)\right|}{\left|H_z^{\text{inc}}(0,z) + H_z^{\text{scat}}(0,z)\right|}\,. \tag{30}$$

5. Single DIE for Conductive Disks

An approximate boundary condition is derived here for purely conductive disks.

The Mitzner GBCs allow for exact representation of the screen of infinite extent in a spectral-domain equivalent transmission line (TL) as a T network, as shown in Figure 2 [35]. The expressions of the longitudinal impedance Z_L and the transverse impedance Z_T are respectively

$$Z_L = \eta_0 \hat{Z}_L = j\eta_0 \zeta_{cr} \tan\left(\frac{k_c d}{2}\right),$$
$$Z_T = \eta_0 \hat{Z}_T = -j\eta_0 \frac{\zeta_{cr}}{\sin(k_c d)}.$$

(31)

When a loop source radiates in the presence of the infinite screen, the equivalent TL of the problem in a Schelkunoff approach [34,36] is as reported in Figure 3, where Z_{loop} is the impedance of the current loop and Z_0 is the free-space impedance η_0.
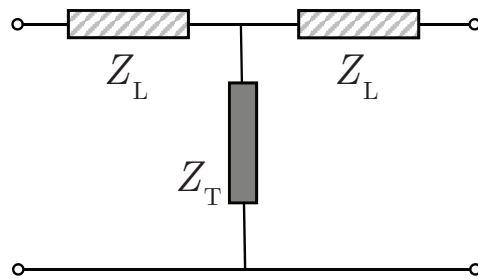
Figure 2. T network representing a thick infinite screen in a spectral-domain TL.
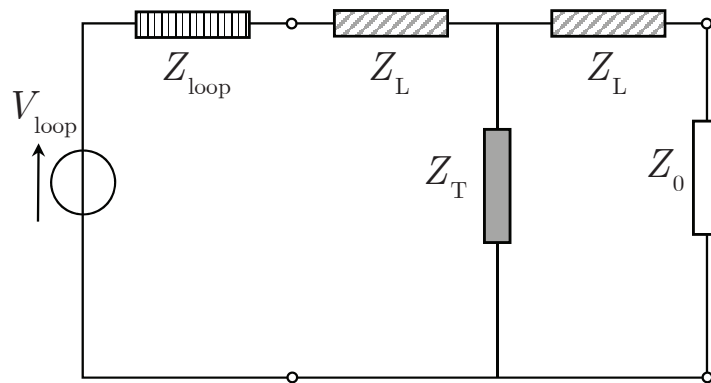

Figure 3. Equivalent TL for a loop radiating in the presence of an infinite screen of finite thickness.

For a magneto-conductive screen, this always results in $|Z_L| \ll Z_0$, and the presence of the longitudinal impedances Z_L in the TL network in Figure 3 can be neglected if the result is $|Z_L| \ll |Z_{loop}|$. The impedance of a parallel loop is a function of the distance; in particular, at the air-screen interface for a small loop, it results in [34,37]

$$Z_{loop} \simeq j\eta_0 \frac{k_0 h}{3}.$$

(32)

Therefore, the effects of Z_L can be neglected if

$$\left| \zeta_{cr} \tan\left(\frac{k_c d}{2}\right) \right| \ll \frac{k_0 h}{3}.$$

(33)

Thus, it should be noted that for purely conducting screens (33) is always satisfied provided that $d \ll h$, which always occurs in practice.

If the presence of the longitudinal impedances Z_L can be neglected, then the screen is represented only by the transverse impedance Z_T. This results in only one boundary condition,

$$\frac{1}{2}\left(\mathbf{E}_{t+} + \mathbf{E}_{t-}\right) = Z_T \mathbf{u}_z \times \left(\mathbf{H}_{t+} - \mathbf{H}_{t-}\right) = Z_T \mathbf{J}_S, \tag{34}$$

which is the same as in (1). Thus, we can derive a single set of DIEs which solves the problem, which consists of (5) and (6) with $i = 1$ and $\hat{Z}_T$ instead of $\hat{Z}_S$. Therefore, under assumption (33), the solution of the original problem requires the introduction of only one unknown (i.e., an equivalent surface electric current density) and the solution of *only one* set of DIEs; this is exactly the same formulation adopted to solve the problem under the assumption of thin screens [16,23]. In such a case, the scattered magnetic field is provided by (24), with coefficients $\psi_n^{(1)}$ provided by the solution of (13) with $i = 1$. Thus, it is clear that with respect to the full formulation based on Mitzner GBCs, the savings in terms of computation time are about 75%.

Another important advantage is that for $k_0 a \ll 1$ (a condition which in practice is always met in EMC) the elements of the matrix (18) have an exceptionally simple expression. In fact, using the series expression derived in [38] to express the integral term in (18), we have

$$A_{mn}^{(1)} \simeq \frac{\hat{Z}_T}{4m}\delta_{mn} + \frac{k_0 a}{8}(-1)^{1-p}\sum_{l=1}^{\infty}\frac{(-j)^l\Gamma\left(p-\frac{l}{2}\right)\Gamma\left(q-\frac{l}{2}\right)(k_0 a)^l}{\Gamma\left(p+1+\frac{l}{2}\right)\Gamma\left(q+1+\frac{l}{2}\right)\Gamma\left(-\frac{l}{2}\right)\Gamma\left(1-\frac{l}{2}\right)} \tag{35}$$

where $\Gamma(\cdot)$ is the Gamma function [33], $p = m - n$, and $q = m + n$. However, for $k_0 a \ll 1$, only one addend is sufficient to reach convergence, such that

$$A_{mn}^{(1)} \simeq \frac{\hat{Z}_T}{4m}\delta_{mn} + j\frac{(k_0 a)^2}{16\pi}\frac{\Gamma\left(p-\frac{1}{2}\right)\Gamma\left(q-\frac{1}{2}\right)}{\Gamma\left(p+\frac{3}{2}\right)\Gamma\left(q+\frac{3}{2}\right)}. \tag{36}$$

Using the definitions of p and q and the properties of the recursive properties of the Gamma function, we finally have

$$A_{mn}^{(1)} \simeq \frac{\hat{Z}_T}{4m}\delta_{mn} + \frac{j}{8\pi}\frac{(k_0 a)^2}{\left[2(m^2-n^2)^2 - (m^2+n^2) + 1\right]}, \tag{37}$$

which makes the solution of the system dramatically faster.

Finally, by following the same line of reasoning as in [24], the linear system (13) with coefficient matrix (37) can be shown to define a Fredholm operator (in particular, a second-kind Fredholm equation) in the space of square-summable sequences, to which the right-hand side of (13) belongs. Hence, the system (13) has a unique solution and guaranteed convergence, and no regularization scheme is required [39].

6. Numerical Results

We first consider a copper disk (conductivity $\sigma = 5.7 \times 10^7$ S/m) with thickness $d = 1$ mm and radius $a = 1.5$ m in a frequency range from 100 Hz to 1 MHz. The electromagnetic source consisting of a circular current loop coaxial with the disk is assumed to be placed at height $h = 30$ cm (i.e., $h/a = 0.2$) and with a radius $R = 5$ cm (i.e., $R \ll a$). In Figure 4, the magnetic shielding effectiveness SE_H is evaluated at a symmetric point with respect to the loop position, i.e., at $z = -h$, and is reported as a function of the frequency.

We have used different formulations here; in particular, it can be seen that the formulation based on Mitzner GBCs (see Section 4, *blue solid line*) is perfectly superimposed with respect to the proposed formulation based on the new boundary condition (34) (see Section 5, *cyan dashed-square line*) in the entire frequency range; these results coincide with those obtained with FEKO commercial software (not reported here).

On the other hand, the formulation based on the thin-screen approximation [23] (*red dashed line*) is correct only up to about 5 kHz; in this low frequency range, the SE_H is essentially that of an infinite metallic screen having the same thickness of the disk [18–20], which is reported in Figure 4 as a dot-dashed line for a fair comparison. In practice, at low frequencies and for the considered values of R and a the metallic disk is seen by the loop as if it were of infinite extent.

At high frequencies (that is, larger than 100 kHz), all the formulations (i.e., the full Mitzner BC formulation, the new proposed BC formulation, the thin-screen formulation, and FEKO) approach the PEC disk results [14], which are shown in Figure 4 as a dotted line.

However, it can clearly be seen that there exists an intermediate frequency range in which neither the thin disk formulation nor the infinite metallic disk formulation can reproduce the correct results. In such a frequency range, the finite thickness of the disk must be carefully taken into account either through the formulation based on Mitzner GBCs or the new boundary condition (34). It can be observed that in this intermediate frequency range the SE_H of the infinite solid conductive thick screen and the SE_H of the infinitesimally thin PEC disk are comparable; moreover, the SE_H of the thick disk with finite conductivity can be much larger (almost 30 dB larger) than the SE_H of the equivalent PEC disk, presenting a sharp peak.

In Figure 5, the dependence of SE_H on the thickness-to-skin depth ratio d/δ is reported for the same parameters as in Figure 4. As expected, the thin disk formulation is accurate only for disk thicknesses smaller than the skin depth δ. Moreover, in this low-frequency range there is no difference with the infinite solid conductive thick screen.
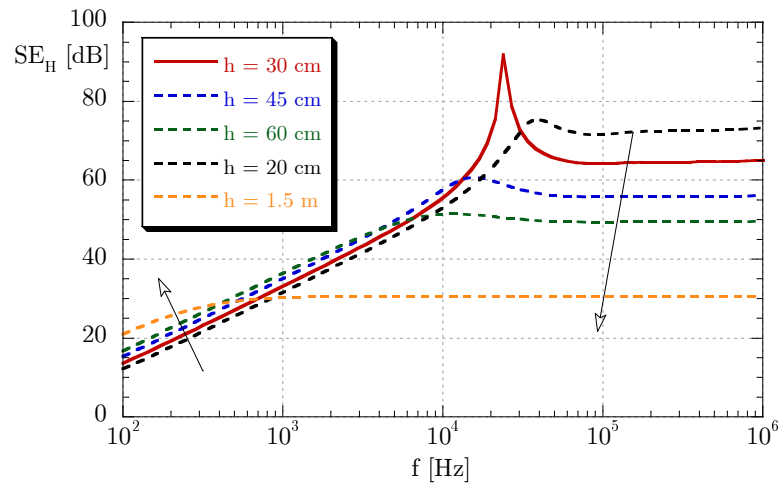
The dependence of SE_H on the on the source-to-screen distance h is instead shown in Figure 6. The distance h ranges from $h = 20$ cm (i.e., $h/a = 0.13$) to $h = 1.5$ m (i.e., $h/a = 1$). Thus, it can be seen that a peak of SE_H may or may not be present in the intermediate frequency range, depending on h; furthermore, the asymptotic PEC limit is approached faster as h increases. Therefore, the presence of the intermediate frequency range with the presence of the SE_H peak is strongly dependent on the source-to-screen distance h. It is interesting to point out that at low frequencies the SE_H increases for larger values of h, while in the high-frequency range the SE_H dramatically decreases with increasing h.
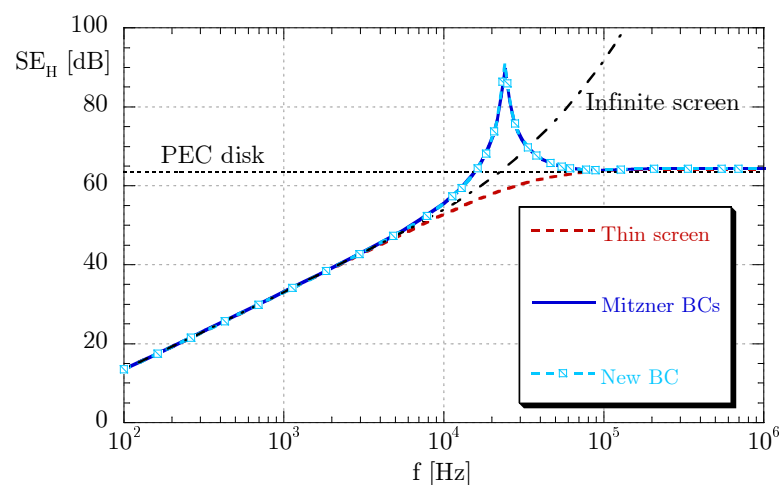
Figure 4. Magnetic shielding effectiveness SE_H as a function of frequency for a purely conductive disk with parameters $d = 1$ mm, $a = 1.5$ m, and $\sigma = 5.7 \times 10^6$ S/m (copper). The coaxial circular current loop source has a radius $R = 5$ cm and is placed at a distance $h = 30$ cm from the disk. The magnetic field is sampled along the z axis at $z = -30$ cm.
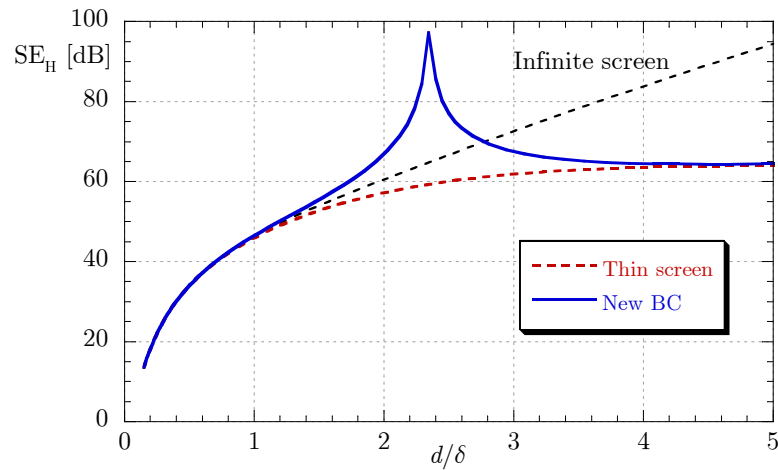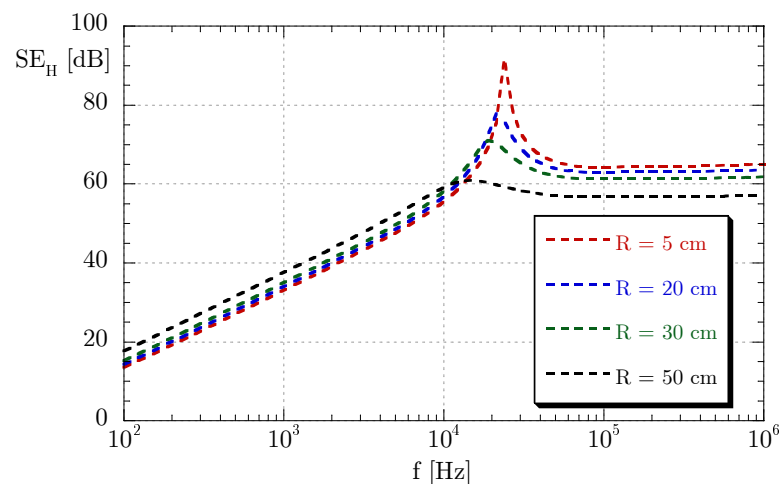
Figure 5. Magnetic shielding effectiveness SE$_H$ as a function of the thickness-to-skin depth ratio d/δ. The other parameters are the same as in Figure 4.

Figure 6. Magnetic shielding effectiveness SE$_H$ as a function of the source-to-screen distance h. The other parameters are the same as in Figure 4.

Finally, the dependence of SE$_H$ on the loop radius R is reported in Figure 7 for radius values between $R = 5$ cm and $R = 50$ cm. While this always results in $R < a$, the loop radius can be smaller or larger than the fixed source-to-screen distance $h = 30$ cm. In all of the cases shown here, the PEC limit is achieved at frequencies higher than about 100 KHz; however, the position and shape of the SE$_H$ peak in the intermediate range depends on R, becoming more pronounced and shifting towards high frequencies as R decreases. On the other hand, at the limit of large R the peak of SE$_H$ tends to disappear.

In summary, in the above figures the variations of SE$_H$ with frequency, thickness-to-skin-depth ratio, source-to-screen distance, and loop radius are illustrated. Although these results do not span the entire parametric space, they are both relevant and representative of the typical electromagnetic response of the considered configuration. Thus, it is worthwhile to point out that although we have considered only copper as a typical conductive material, the validity of the method is general and has been tested on different values of the disk conductivity.

Figure 7. Magnetic shielding effectiveness SE$_H$ as a function of the loop radius R. The other parameters are the same as in Figure 4.

7. Conclusions

The magnetic shielding effectiveness of a finite screen consisting of a circular disk with finite conductivity and finite thickness is evaluated when a circular current loop of finite radius coaxial with the disk and with constant current is assumed as the electromagnetic field source. An original formulation is proposed to solve the problem using suitable generalized boundary conditions to take into account the finite thickness of the screen and solving the two dual integral equations derived by enforcing the boundary conditions through an expansion of the unknowns in Neumann series of Bessel functions. An alternative formulation that is valid for a purely conductive screen with no magnetic properties is proposed as well, and is computationally much faster. The magnetic shielding effectiveness is studied in different configurations while pointing out possible critical situations. Additional work is currently in progress to extend the presented analysis to non-constant exciting currents.

References

1. Bouwkamp, C.J. On the diffraction of electromagnetic waves by small circular disks and holes. *Philips Res. Rep.* **1950**, *5*, 401–422.
2. Flammer, C. The vector wave function solution of the diffraction of electromagnetic waves by circular disks and apertures. I. Oblate spheroidal vector wave functions. *J. Appl. Phys.* **1953**, *24*, 1218–1223. [CrossRef]
3. Eggimann, W.H. Higher-order evaluation of electromagnetic diffraction by circular disks. *IRE Trans. Microw. Theory Techn.* **1961**, *9*, 408–418. [CrossRef]
4. Williams, W.E. Electromagnetic diffraction by a circular disk. In *Mathematical Proceedings of the Cambridge Philosophical Society*; Cambridge University Press: Cambridge, UK, 1962; Volume 58, pp. 625–630.
5. Marsland, D.; Balanis, C.; Brumley, S. Higher order diffractions from a circular disk. *IEEE Trans. Antennas Propag.* **1987**, *35*, 1436–1444. [CrossRef]

6. Duan, D.W.; Rahmat-Samii, Y.; Mahon, J.P. Scattering from a circular disk: A comparative study of PTD and GTD techniques. *Proc. IEEE* **1991**, *79*, 1472–1480. [CrossRef]
7. Hongo, K.; Naqvi, Q.A. Diffraction of electromagnetic wave by disk and circular hole in a perfectly conducting plane. *Prog. Electromagn. Res.* **2007**, *68*, 113–150. [CrossRef]
8. Hongo, K.; Jafri, A.D.U.; Naqvi, Q.A. Scattering of electromagnetic spherical wave by a perfectly conducting disk. *Prog. Electromagn. Res.* **2012**, *129*, 315–343. [CrossRef]
9. Kaloshin, V.A.; Klionovski, K.K. Scattering of dipole field by perfectly conducting disk. *J. Radio Electr.* **2013**, *12*, 1–23.
10. Peterson, A.F.; Bibby, M.M. Electromagnetic scattering from a disk: Use of Flammer's solution to assess numerical techniques incorporating singular expansions. *IEEE Trans. Antennas Propag.* **2018**, *67*, 616–621. [CrossRef]
11. Jiao, C.; Yang, X.; Qi, L. Low-frequency magnetic shielding of a perfectly electric conducting circular disk: Approximately analytical formulation considering radius of emitting loop. *IEEE Trans. Electromagn. Compat.* **2022**, *64*, 897–901. [CrossRef]
12. Di Murro, F.; Lucido, M.; Panariello, G.; Schettino, F. Guaranteed-convergence method of analysis of the scattering by an arbitrarily oriented zero-thickness PEC disk buried in a lossy half-space. *IEEE Trans. Antennas Propag.* **2015**, *63*, 3610–3620. [CrossRef]
13. Lucido, M.; Panariello, G.; Schettino, F. Scattering by a zero-thickness PEC disk: A new analytically regularizing procedure based on Helmholtz decomposition and Galerkin method. *Radio Sci.* **2017**, *52*, 2–14. [CrossRef]
14. Lovat, G.; Burghignoli, P.; Araneo, R.; Celozzi, S.; Andreotti, A.; Assante, D.; Verolino, L. Shielding of a perfectly conducting disk: Exact and static analytical solution. *Prog. Electromagn. Res. C* **2019**, *95*, 167–182. [CrossRef]
15. Balaban, M.V.; Sauleau, R.; Benson, T.M.; Nosich, A.I. Dual integral equations technique in electromagnetic wave scattering by a thin disk. *Prog. Electromagn. Res.* **2009**, *16*, 107–126. [CrossRef]
16. Lucido, M.; Schettino, F.; Panariello, G. Scattering from a thin resistive disk: A guaranteed fast convergence technique. *IEEE Trans. Antennas Propag.* **2021**, *69*, 387–396. [CrossRef]
17. Lucido, M.; Balaban, M.V.; Nosich, A.I. Plane wave scattering from thin dielectric disk in free space: Generalized boundary conditions, regularizing Galerkin technique and whispering gallery mode resonances. *IET Microw. Antennas Propag.* **2021**, *15*, 1159–1170. [CrossRef]
18. Lovat, G.; Burghignoli, P.; Araneo, R.; Celozzi, S. Magnetic shielding of planar metallic screens: A new analytical closed-form solution. *IEEE Trans. Electromagn. Compat.* **2020**, *62*, 1884–1888. [CrossRef]
19. Lovat, G.; Burghignoli, P.; Araneo, R.; Stracqualursi, E.; Celozzi, S. Analytical evaluation of the low-frequency magnetic shielding of thin planar magnetic and conductive screens. *IEEE Trans. Electromagn. Compat.* **2021**, *63*, 308–312. [CrossRef]
20. Lovat, G.; Burghignoli, P.; Araneo, R.; Celozzi, S. Exact closed-form shielding effectiveness of planar screens with small parallel loops. *IEEE Trans. Electromagn. Compat.* **2022**, *64*, 1694–1702. [CrossRef]
21. Burghignoli, P.; Lovat, G.; Araneo, R.; Celozzi, S. Pulsed vertical dipole response of a thin sheet with high-contrast dielectric and conductive properties. *IEEE Trans. Antennas Propag.* **2017**, *66*, 217–225. [CrossRef]
22. Burghignoli, P.; Lovat, G.; Araneo, R.; Celozzi, S. Time-domain shielding of a thin conductive sheet in the presence of vertical dipoles. *IEEE Trans. Electromagn. Compat.* **2018**, *60*, 157–165. [CrossRef]
23. Lovat, G.; Burghignoli, P.; Araneo, R.; Celozzi, S.; Andreotti, A.; Assante, D.; Verolino, L. Shielding of an imperfect metallic thin circular disk: Exact and low-frequency analytical solution. *Prog. Electromagn. Res.* **2020**, *167*, 1–10. [CrossRef]
24. Lovat, G.; Burghignoli, P.; Araneo, R.; Celozzi, S. Axially symmetric source field penetration through a circular aperture in a thin impedance plate. *IEEE Trans. Antennas Propag.* **2022**, *70*, 8348–8359. [CrossRef]
25. Mitzner, K. Effective boundary conditions for reflection and transmission by an absorbing shell of arbitrary shape. *IEEE Trans. Antennas Propag.* **1968**, *16*, 706–712. [CrossRef]
26. Karlsson, A. Approximate boundary conditions for thin structures. *IEEE Trans. Antennas Propag.* **2009**, *57*, 144–148. [CrossRef]
27. Sukharevsky, I.O.; Shapoval, O.V.; Altintas, A.; Nosich, A.I. Validity and limitations of the median-line integral equation technique in the scattering by material strips of sub-wavelength thickness. *IEEE Trans. Antennas Propag.* **2014**, *62*, 3623–3631. [CrossRef]
28. Lovat, G.; Araneo, R.; Celozzi, S.; Burghignoli, P. Magnetic shielding of a thick circular conductive disk against a coaxial current loop. In Proceedings of the 2022 Microwave Mediterranean Symposium (MMS), Pizzo Calabro, Italy, 9–13 May 2022; pp. 1–4.
29. Shapoval, O.V.; Sauleau, R.; Nosich, A.I. Scattering and absorption of waves by flat material strips analyzed using generalized boundary conditions and Nystrom-type algorithm. *IEEE Trans. Antennas Propag.* **2011**, *59*, 3339–3346. [CrossRef]
30. Lucido, M.; Balaban, M.V.; Dukhopelnykov, S.; Nosich, A.I. A fast-converging scheme for the electromagnetic scattering from a thin dielectric disk. *Electronics* **2020**, *9*, 1451. [CrossRef]
31. Lovat, G.; Burghignoli, P.; Araneo, R.; Celozzi, S. Magnetic-field transmission through a circular aperture in a magneto-conductive screen: Identification of aperture penetration and field diffusion contributions. *IEEE Trans. Electromagn. Compat.* **2023**, *submitted*.
32. Gradshteyn, I.S.; Ryzhik, I.M. *Table of Integrals, Series, and Products*, 7th ed.; Academic Press: Burlington, MA, USA, 2014.
33. Abramowitz, M.; Stegun, L.A. *Handbook of Mathematical Functions*; Dover Publications Inc.: New York, NY, USA, 1972.
34. Celozzi, S.; Araneo, R.; Burghignoli, P.; Lovat, G. *Electromagnetic Shielding*, 2nd ed.; IEEE Wiley: Hoboken, NJ, USA, 2022.
35. Tretyakov, S. *Analytical Modeling in Applied Electromagnetics*; Artech House: Norwood, MA, USA, 2003.
36. Schelkunoff, S.A. The impedance concept and its application to problems of reflection, refraction, shielding and power absorption. *Bell Syst. Tech. J.* **1938**, *17*, 17–48. [CrossRef]
37. Whitehouse, A.C.D. Screening: New wave impedance for the transmission-line analogy. *Proc. IEE* **1969**, *116*, 1159–1164. [CrossRef]

38. Lovat, G.; Burghignoli, P.; Araneo, R.; Celozzi, S. Magnetic field penetration through a circular aperture in a perfectly conducting plate excited by a coaxial loop. *IET Microw. Antennas Propag.* **2021**, *15*, 1147–1158. [CrossRef]

39. Nosich, A.I. The method of analytical regularization in wave-scattering and eigenvalue problems: Foundations and review of solutions. *IEEE Antennas Propag. Mag.* **1999**, *41*, 34–49. [CrossRef]